REPORT DOCUMENTATION PAGE	Form Approved OMB NO. 0704-0188

The public reporting burden for this collection of information is estimated to average 1 hour per response, including the time for reviewing instructions, searching existing data sources, gathering and maintaining the data needed, and completing and reviewing the collection of information. Send comments regarding this burden estimate or any other aspect of this collection of information, including suggesstions for reducing this burden, to Washington Headquarters Services, Directorate for Information Operations and Reports, 1215 Jefferson Davis Highway, Suite 1204, Arlington VA, 22202-4302. Respondents should be aware that notwithstanding any other provision of law, no person shall be subject to any oenalty for failing to comply with a collection of information if it does not display a currently valid OMB control number.
PLEASE DO NOT RETURN YOUR FORM TO THE ABOVE ADDRESS.

1. REPORT DATE (DD-MM-YYYY)	2. REPORT TYPE	3. DATES COVERED (From - To)
29-11-2017	Final Report	14-Jun-2016 - 31-Aug-2017

4. TITLE AND SUBTITLE	5a. CONTRACT NUMBER
Final Report: Ultracompact, High-Speed Field-Effect Optical Modulators(Research Topic 4.2 Optoelectronics)	W911NF-16-1-0357
	5b. GRANT NUMBER
	5c. PROGRAM ELEMENT NUMBER 611102
6. AUTHORS	5d. PROJECT NUMBER
	5e. TASK NUMBER
	5f. WORK UNIT NUMBER

7. PERFORMING ORGANIZATION NAMES AND ADDRESSES	8. PERFORMING ORGANIZATION REPORT NUMBER
Rochester Institute of Technology 141 Lomb Memorial Drive Rochester, NY 14623 -5603	

9. SPONSORING/MONITORING AGENCY NAME(S) AND ADDRESS (ES)	10. SPONSOR/MONITOR'S ACRONYM(S)
U.S. Army Research Office P.O. Box 12211 Research Triangle Park, NC 27709-2211	ARO
	11. SPONSOR/MONITOR'S REPORT NUMBER(S) 68775-EL.1

12. DISTRIBUTION AVAILIBILITY STATEMENT

Approved for public release; distribution is unlimited.

13. SUPPLEMENTARY NOTES

The views, opinions and/or findings contained in this report are those of the author(s) and should not contrued as an official Department of the Army position, policy or decision, unless so designated by other documentation.

14. ABSTRACT

15. SUBJECT TERMS

16. SECURITY CLASSIFICATION OF:			17. LIMITATION OF ABSTRACT	15. NUMBER OF PAGES	19a. NAME OF RESPONSIBLE PERSON
a. REPORT	b. ABSTRACT	c. THIS PAGE			Karl Hirschman
UU	UU	UU	UU		19b. TELEPHONE NUMBER 000-000-0000

Standard Form 298 (Rev 8/98)
Prescribed by ANSI Std. Z39.18

RPPR Final Report
as of 05-Dec-2017

Agency Code:

Proposal Number: 68775EL | **Agreement Number: W911NF-16-1-0357**

INVESTIGATOR(S):

Name: Karl Hirschman
Email: kdhemc@rit.edu
Phone Number: 0000000000
Principal: Y

Organization: **Rochester Institute of Technology**
Address: 141 Lomb Memorial Drive, Rochester, NY 146235603
Country: USA
DUNS Number: 002223642 EIN:

Report Date: 30-Nov-2017 Date Received: 29-Nov-2017
Final Report for Period Beginning 14-Jun-2016 and Ending 31-Aug-2017
Title: Ultracompact, High-Speed Field-Effect Optical Modulators(Research Topic 4.2 Optoelectronics)
Begin Performance Period: 14-Jun-2016 **End Performance Period:** 31-Aug-2017
Report Term: 0-Other

Submitted By: Karl Hirschman Email: kdhemc@rit.edu
Phone: (000) 000-0000

Distribution Statement: 1-Approved for public release; distribution is unlimited.

STEM Degrees: 1 **STEM Participants:** 2

Major Goals: The major goals of the project include two parts. First, an ultracompact plasmonic electro-optical (EO) modulator was to be developed and investigated for efficient intensity modulation. Second, an ultracompact and high-speed EO modulator based on a dielectric platform was to be developed for straightforward integration with existing CMOS technology. Both modulators were targeted to facilitate next-generation interconnects for integrated photonic circuits.

Accomplishments: Note: Please see the uploaded pdf document for a more complete description on the following details regarding project accomplishments.

This work explored novel conductive oxide-based slot waveguides based on the unique properties of indium-tin-oxide (ITO). This research was one of the first experimental attempts to demonstrate optical modulators at nanoscale, and one of the first systematic explorations of conductive oxide-based modulation at GHz level. The research results contribute towards the advancement of nanophotonic technology and on-chip optical interconnects, and will support fundamental theory and techniques for field-effect electro-absorption modulators.

Ultra-compact field effect plasmonic modulator

In this project, a metal-insulator-conductive oxide-insulator-metal (MICIM) waveguide was proposed and investigated. We showed that light absorption in the gap between two gold films is controlled by the electric-field-induced charge in an intermediate ITO layer. The MICIM structure may be biased such that the ITO layer is either in electron depletion or accumulation, thus changing the absorption of the waveguide. Thus the structure can switch between high and low absorptive states. MICIM modulators were designed and fabricated, consisting of a series of layer-by-layer processes. Photolithography, thin film deposition, and lift-off processes were used for precise pattern definitions. Modulators of different waveguide lengths as small as 800 nm were characterized. The modulation performance of the 800 nm (length) modulator was measured with a DC-coupled photodetector using an applied 14 Vpp RF sine wave at 10 MHz, with a resulting extension ratio of 3.04 dB/?m. An AC-coupled photodetector was used to demonstrate modulator operation at frequencies up to 500 MHz.

Ultra-compact high-speed dielectric modulator

The project also investigated a doped Si-ITO-HfO_2 dielectric modulator, which can provide straightforward photonic integration. In this device, TiO_2 serves as a dielectric slot waveguide for guiding light to interact with ITO. External electric signals are applied on n+ doped Si and ITO electrodes, which stimulates the field effects in the active ITO

layer at the ITO-HfO2 interface. The device was fabricated on SOI substrates. Gratings on the U-shaped waveguide ends were used for light coupling from angled fiber arrays. Gold was used for electrical contact pads. The coupling efficiency was measured to be relatively low, with a peak value of 2% at 1510 nm. For comparison, the FDTD simulation results based on the measured film parameters of the fabricated device resulted in a peak 5.5% output transmission at the wavelength of 1510 nm. An AC modulation depth of 2.5 dB/?m was realized on an 8 ?m long modulator waveguide at 100 MHz. The modulation depth decays with increasing frequency, showing that the device has a RC circuit-limited operation speed. Nevertheless, successful modulation at frequencies as high as 2 GHz was demonstrated.

Training Opportunities: The students involved in associated R&D activities have been exposed to a wide variety of technologies in electro-optic device design and simulation, nanofabrication, metrology, and electrical/optical device characterization. Students have gained invaluable experience in these areas at laboratories both at RIT and at the NSF Nanofabrication facility at Cornell University. This experience will serve them well as they either enter the workforce in a related technical field or perhaps remain in an academic research environment.

Results Dissemination: Conference presentation:
K. Shi, and Z. Lu, "Ultracompact field-effect plasmonic modulator," FIO, FTu3D. 2, Oct 2016.

Journal articles (In preparation):
K. Shi, P. Yin, Z. Lu, K. Hirschman, and S. Preble, "An ultracompact plasmonic electro-absorption modulator with MHz operation," In preparation.
K. Shi, P. Yin, Z. Lu, K. Hirschman, and S. Preble, "Compact and high-speed Indium Tin Oxide (ITO)-based electro-absorption modulator on a dielectric platform," In preparation.

Honors and Awards: Nothing to Report

Protocol Activity Status:

Technology Transfer: Nothing to Report

PARTICIPANTS:

Participant Type: PD/PI
Participant: Karl D. Hirschman
Person Months Worked: 1.00 **Funding Support:**
Project Contribution:
International Collaboration:
International Travel:
National Academy Member: N
Other Collaborators:

Participant Type: Co PD/PI
Participant: Stefan Preble
Person Months Worked: 1.00 **Funding Support:**
Project Contribution:
International Collaboration:
International Travel:
National Academy Member: N
Other Collaborators:

Participant Type: Graduate Student (research assistant)
Participant: Kaifeng Shi
Person Months Worked: 15.00 **Funding Support:**
Project Contribution:
International Collaboration:
International Travel:

National Academy Member: N
Other Collaborators:

Ultra-compact, High-Speed Field Effect Electro-Optical Modulators

Kaifeng Shi[*], Karl Hirschman[*,†] and Stefan Preble[*,†]

[*]*Microsystems Engineering PhD Program*
[†]*Department of Electrical and Microelectronic Engineering*
Rochester Institute of Technology, Rochester, New York, 14623, USA

Abstract

One of the technical barriers impeding the wide applications of integrated photonic circuits is the lack of ultracompact, high speed, broadband electro-optical (EO) modulators, which up-convert electronic signals into high bit-rate photonic data. In addition to direct modulation of lasers, EO modulators can be classified into (i) phase modulation based on EO effect or free-carrier injection [1, 2], or (ii) absorption modulation based on Franz-Keldysh effect or quantum-confined Stark effect [3- 7]. Due to the poor EO properties of regular materials, a conventional EO modulator has a very large footprint. Based on high-Q resonators, recent efforts have advanced EO modulators [8,9,10] into microscale footprints, which have nearly reached their physical limits restricted by the materials. On-chip optical interconnects require ultrafast EO modulators at the nanoscale. The technical barrier may not be well overcome based on conventional approaches and well-known materials. Herein, we theoretically demonstrated the possibility of realizing nanoscale EO, more specifically electro-absorption (EA) modulators based on the integration of novel yet inexpensive materials, conductive oxides (COs), in a metal-oxide-semiconductor (MOS)-like waveguide plasmonic or dielectric platform [11]. Our experimental investigation verified the feasibility of the proposed modulators, and showed that the EA modulation was induced by field effect in the MOS-like structure, which is enhanced by high-k insulator, HfO_2 [12,13]. By utilizing a metal-insulator-CO-insulator-metal (MICIM) structure with double-capacitor gating scheme, we successfully demonstrated an ultra-compact field effect plasmonic EA modulator with waveguide length of only 800 nm, which is the smallest recorded dimension according to our knowledge [14]. Measurements show that it has an extinction ratio of 3.04 dB/μm at 10 MHz, and works up to 500 MHz. Furthermore, we explored a doped Si-insulator-CO field effect EA modulator based on silicon-on-insulator (SOI) dielectric platform. The dielectric modulator has an ultra-compact footprint of 4 μm^2, and exhibits up to 2 GHz operation speed at telecommunication wavelengths.

1. Ultra-compact field effect plasmonic modulator

1.1 Background and design

Most of previous effort was focused on the exploration of the EO properties of dielectrics or polymers owing to their low optical absorption for waveguide applications, whereas the optical properties of absorptive materials, for example conducting oxides (COs), have been relatively overlooked, until recent work showing that the optical dielectric constant of COs in the charged layer of a metal-insulator-CO (MIC) structure can be tuned in a large range by electrical gating [15]. When a large electric field is applied across the insulator layer of an MIC structure, significant surface charge can be induced and the induced charge can greatly alter the optical properties at the insulator-CO interface. In this sense, COs are good active materials for EO modulation. Indeed, many EO modulators have been proposed based on COs as the active material [16,17,18,19,20,21]. To apply a CO as active medium in an EO modulator, one challenge is that the field-effect-induced charge layer is only few nanometers thick. To enhance the impact of the charged layer on light absorption, three strategies are taken in this work.

First, the CO is integrated into an MIM plasmonic waveguide. Surface plasmons as hybrid electrical-optical waves give rise to strong confinement, which makes their propagation to be extremely sensitive to minor changes in the optical properties of the guiding materials. This provides a remarkable opportunity for optical modulation. Various plasmonic EO modulators have been reported since the 1980s [22,23,24,25,26], including three based on COs [12,27,28]. In particular, Dionne, et al. [26] reported an EO modulator integrating a metal-oxide-silicon junction into two silver films, where the modulating electric field can switch the waveguide between guiding and cut-off states. However, its large extinction ratio extremely relies on the junction uniformity in the light propagation direction. Two more recent works from another group reported microscale plasmonic phase modulator [29] and plasmonic intensity modulator [30]. In both works, MIM plasmonic waveguides are employed and nonlinear polymers work as the active media with modulator waveguide length shrunk to 10s of micrometers. Recent experimental works [12,27,28] report the integration of the MIC structure on the silicon waveguide, in a plasmonic waveguide, and below a glass prism, respectively. Modulation extinct ratio is reported 1 dB/μm in Ref. [27], and 2.71 dB/μm in Ref. [28]. In both cases, the dynamical operation of the modulators has not been reported. The result from Ref. [12] shows that the part

of large modulation may only work at low speed. Whether the modulation can work at high speed is still a question.

Second, HfO_2 is employed as the insulator layer to enhance the field effect. HfO_2 has high DC dielectric constant, large dielectric strength, and is transparent for NIR light. Basically, the MIC structure functions as a parallel plate capacitor. Thus, a high-k insulator can induce large surface charge for a given gate voltage.

Third, two MIC structures are designed back-to-back to double the field-induced charge, simultaneously on top and bottom sides of CO, for the same gate voltage. The use of this double capacitor gating scheme in modulators can date back to dual-channel EO modulators proposed in 1970s or earlier [31]. It was recently used in a graphene modulator [32] and a proposed silicon slot-waveguide-based EO modulator [33]. The entire structure in this work is thus a metal-insulator-CO-insulator-metal (MICIM) structure, as shown in Fig. 1(a). The CO used in this work is ITO. Another advantage of using the double insulator layers is to decrease the MIM plasmonic waveguide attenuation, which sharply decreases with the increase of insulator thickness, especially at the nanoscale.

This work shows that the three strategies can greatly improve the modulator performance and result in an EA modulator with a propagation length only 800 nm. To our knowledge, this is the first experimental demonstration of an EO modulator with a nanoscale waveguide length. The EO modulators in previous works [26,27,28,29,30] involve waveguides with nanoscale width or thickness, but the waveguide length is still at the microscale.

1.2 Modeling and fabrication

As shown in Fig. 1 (a-c), the principle of this EO modulator is quite straightforward. Light absorption in the gap between two gold films is controlled by the electric-field-induced charge in the ITO layer. Each MIC structure functions as a parallel plate capacitor. The field induced charge on each side of ITO can be calculated according to $Q = \varepsilon EA$, where ε is the DC dielectric constant of HfO_2, E is the applied electric field across the HfO_2 layer, and A is the capacitor area. According to the bias polarity and strength, an MIC structure may work in two well-known modes. When a positive bias is applied at the ITO layer, depletion (of electrons) ($Q > 0$) occurs. Effectively, the thickness of ITO layer decreases and the MICIM waveguide becomes less absorptive, resulting low attenuation (i.e. ON state). When a negative bias is applied at the ITO

layer, accumulation (of more electrons) ($Q < 0$) occurs. The ITO layer becomes more conductive and the MICIM waveguide becomes more absorptive, resulting high attenuation (i.e. OFF state). The third working mode of a metal-oxide-semiconductor structure, inversion (of carriers into holes), is less likely to occur.

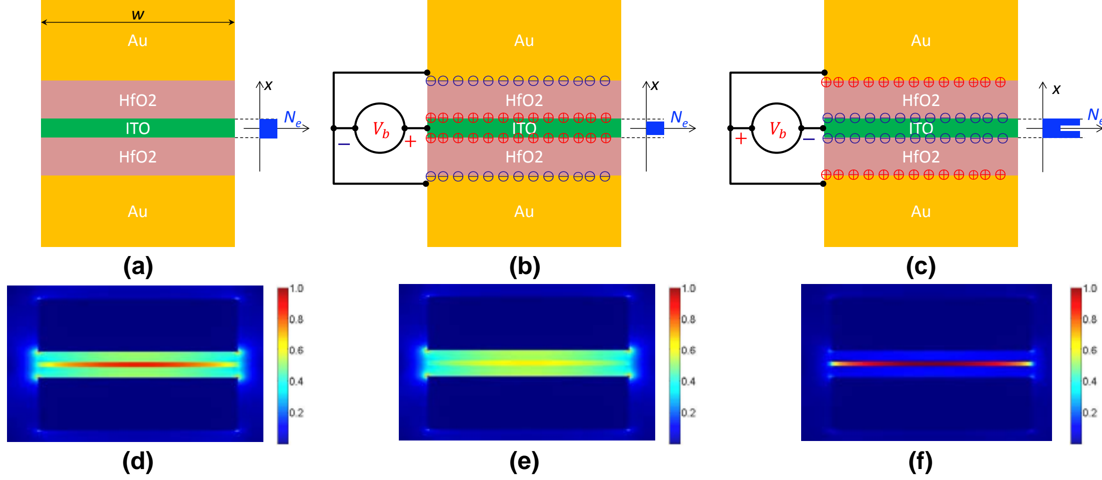

Figure 1. Illustration of the working modes of the metal-insulator-CO-insulator-metal structure: (a) Without bias. (b) Depletion mode, where the ITO is less absorptive and the waveguide has lower attenuation. (c) Accumulation mode, where the ITO is more absorptive and the waveguide has higher attenuation. (d) The mode profile for the no bias case. (e) The mode profile for the depletion case. (f) The mode profile for the accumulation case.

Quantitatively, the optical dielectric constant ϵ of the ITO can be approximated by its free carrier concentration according to the Drude model,

$$\epsilon = \epsilon' + j\epsilon'' = \epsilon_\infty - \frac{\omega_p^2}{\omega(\omega + j\gamma)} \tag{1}$$

where ϵ_∞ is the high frequency dielectric constant, ω_p is the plasma frequency, and γ is the electron damping factor. ϵ' and ϵ'' are real and imaginary parts of optical dielectric constant, respectively. Note plasma frequency $\omega_p = \sqrt{\frac{Nq^2}{\epsilon_o m^*}}$, depending on carrier concentration N, and the effective electron mass m^*. q represents the elementary charge. To make ω_p located in the NIR regime, the carrier concentration, N, should reduce to 10^{20}~10^{22} cm^{-3}, coinciding to that of COs. Outside of the range, the effect of same level of electric-field-induced charge becomes less significant on waveguide attenuation [**Error! Bookmark not defined.**]. The specific value of carrier concentration can be controlled by the growth/deposition processes and post-annealing

conditions [34]. In our work, the thickness of ITO is designed to be 10 nm; each HfO_2 layer is 30 nm thick. Note that thicker insulating layers can result in lower losses of the MICIM waveguide.

The schematic of the device is illustrated in Fig. 2(a). The device fabrication consists of a series of layer-by-layer processes. For accurately patterning each layer, general photolithography and lift-off processes are applied. The fabrication starts from the deposition of 10 nm thick Ti adhesion and 100 nm thick gold layers on quartz substrate. Then, a 20-nm HfO_2 is deposited as the first buffer insulator by atomic layer deposition (ALD). The next process is the sputtering of 10-nm active material, ITO, at a substrate temperature of 60°C. After that, another 20-nm thick HfO_2 is deposited to provide the second buffer layer. Finally, 150-nm thick gold is deposited to define the light input port, the modulator length as well as to form electric contacts.

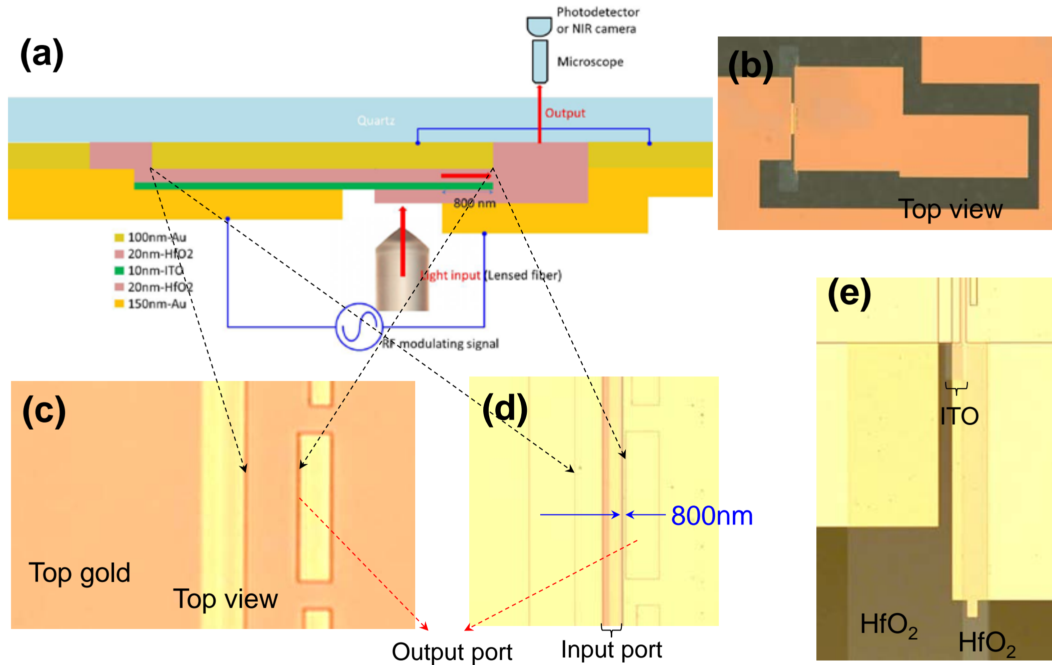

Figure 2. (a) Schematic of the fabricated EO modulator and the test setup. (b) Top view of the modulators and their GSG contact electrodes. (c) Top view of the output port. (c) Bottom view of the device input and output ports. (d) Bottom view of the edge of the device.

To test the device, the sample is flipped upside down as illustrated in Fig. 2(a). For easy description, the quartz substrate is treated as the top layer. As can be seen in Fig. 2 (b, c, d), there are three modulators with waveguide lengths, 3.0 μm, 800 nm, and 2.0 μm, respectively (The prototype MICIM modulator in the proposal of this project only has one output port with a waveguide length of 1.0 μm). The three modulators share the same GSG contact electrodes. Our

investigation is focused on the 800-nm waveguide. Figures 2 (c & d) are the top and bottom side microscope images of our fabricated device. Figure 2(e) is the image of the edge of the device taken from the bottom side showing the multi-layer stacks.

1.3 Light coupling and modulation measurement

In the measurement, due to the relatively high optical losses in the MICIM waveguide, light from a tunable laser is first amplified by an erbium-doped fiber amplifier (EDFA) and then coupled into the sample through a lensed fiber from the bottom side of the sample. The lensed fiber can focus NIR light into a ~2 μm diameter spot at the working distance of ~15 μm. The entire sample is covered by either the top or bottom gold layer, or both layers. For easy explanation, the top and bottom gold layers are shown as slightly different colors. The gold layers are thick enough so that light cannot directly propagate through as shown in Fig. 2(b & c). The input port is a 10 μm wide slit in the bottom gold layer as shown in Fig. 2(d). Light propagation through the sample has to follow the gaps, i.e. plasmonic waveguides, between the two gold layers. See Fig. 2(a). Two MIM plasmonic waveguides simultaneously exist in our modulator. The left side one is an Au-HfO_2-ITO-Au waveguide, which has very large attenuation and its length is designed to be 4 μm. Thus, the light transmission through the Au-HfO_2-ITO-Au waveguide is negligible. The right side one is an Au-HfO_2-ITO-HfO_2-Au waveguide, which is our modulating waveguide. It has much smaller attenuation, owing to the double HfO_2 layers, and much shorter length, only 800 nm, terminated by a slit in the top gold layer, which works as the output port. Therefore, the input and output ports are linked by the Au-HfO_2-ITO-HfO_2-Au waveguide.

As illustrated in Fig. 2(a), the top gold layer seems three separate parts, but the middle and right parts actually represent a continuous film with a 5μm-by-30μm rectangular window (The window dimension was 10μm-by-60μm in the prototype MICIM modulator), as shown in Fig. 2(c), which means the top gold layer only has two electrically insulated parts. The bottom gold layer is also two insulated films: the left part works as a metal contact electrode for ITO; the right part simultaneously works as another electrode and a confining layer of the Au-HfO_2-ITO-HfO_2-Au plasmonic waveguide. As can be seen in Fig. 2(a), two confining gold layers of this waveguide are electrically connected at the right end. Consequently, when a voltage is applied between ITO and bottom gold layer, the same voltage is always applied between ITO and the top gold layer. The result is the double capacitor gating scheme as shown in Fig. 1. The gate voltage

comes from a function generator and is applied to the electrodes through a microwave GSG probe from the sample bottom side. See Fig. 2(b).

In the experiment, a microscope, installed with an NIR camera at the top through an adapter, is placed over the sample for observation, alignment, and NIR imaging. The microscope is first adjusted to locate the output port. Figure 3(a) shows the image of the sample by the NIR camera. Then amplified NIR light (λ = 1560 nm) is fed into the input port through a lensed fiber. After the light propagates through the device, it is scattered into the quartz substrate and then into the air. Partial scattered light is imaged by the microscope NIR camera. Figure 3(b) shows the light scattering from the middle output window.

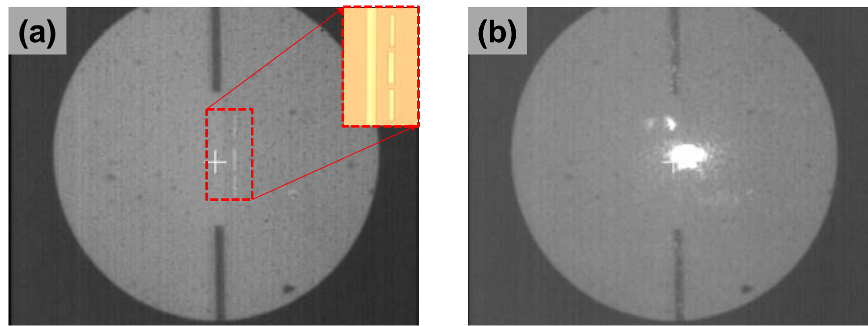

Figure 3. (a) Image of the output ports by the NIR camera. (b) Image of the output of the device through the NIR camera when NIR light is fed in from the input port.

When an AC voltage (14V-Vpp) is applied on the device, the change of power level of the output light with the voltage fluctuation can be observed. This verifies that the light output is really modulated. The modulation is so obvious that light intensity change in the NIR image can easily be seen by eyes at extremely low frequencies (several hertz).

To test response of the device to higher frequency modulating voltage, the NIR camera is first replaced by a DC-coupled InGaAs photodetector (Thorlabs PDA10CF), which is positioned exactly at the focused image of the microscope adapter. The photodetector collects the output light power and converts it into an electric signal in an oscilloscope. A 50-Ω load is used to convert the photocurrent into voltage, V_{op}. Figures 4 (a&b) depict the tested photo voltage of the EA modulator under an applied 14 Vpp RF sine signal of 1 MHz and 10 MHz, respectively. If the extinction ratio (ER) is defined by $r_e = \frac{\max\{V_{op}\}}{\min\{V_{op}\}}$, the ER measured at 10 MHz is around 1.75 or 3.04 dB/μm (The ER for the prototype modulator was ~0.8 dB/μm at 1 MHz). To demonstrate the operation of the modulator at even higher frequency, the DC-coupled photodetector is

replaced by an AC-coupled, amplified InGaAs photodetector (Newport 818-BB-30A), and the output is amplified by a microwave amplifier. Figures 4 (c&d) plot the tested photo voltage of the EA modulator under an applied 14V-Vpp RF sine signal with frequencies f = 100 MHz and f = 500 MHz, respectively.

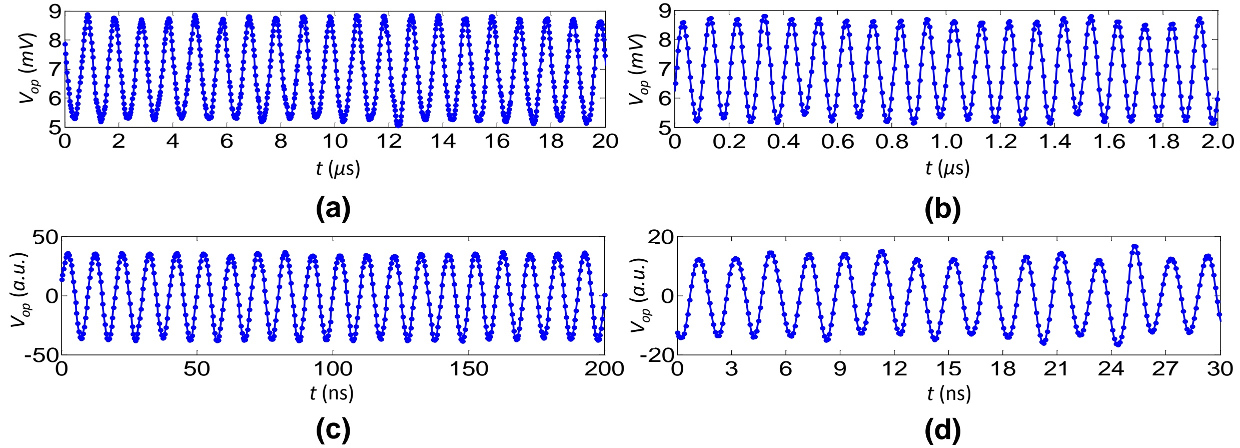

Figure 4. Oscilloscope measurement of the output light power under an applied electric signal of (a) 1 MHz, (b) 10 MHz, (c) 100 MHz, and (d) 500 MHz. (a&b) are obtained using a DC-coupled photodetector. (c&d) are obtained using an AC-coupled photodetector.

1.4 Circuit analysis

In the measurement, we obtained a modulation speed up to 500 MHz, which is a considerable improvement compared with our previous investigations. However, it is still very insufficient to be considered an ultra-fast EO modulator. The speed of the photodetector (bandwidth up to 1.5 GHz), the power level of the incident light, and the input coupling efficiency might be the factors that limit the operation speed of the MICIM plasmonic modulator. However, considering the relatively large modulator waveguide width and contact pads, the device RC constant should be the main constraint for the speed. Therefore, we conducted circuit analysis to examine the RC delay of the device.

A high speed (20 GHz) network analyzer is used for the analysis. In Fig. 5(a), we plot the RF reflection coefficient S_{11} of the device circuit as a function of frequency. We can see S_{11} value drops to -3dB at ~300MHz, and bounces back at higher frequencies, which indicates that the device circuit turns from capacitive to inductive due to the existence of parasitic inductance. As a result, we treat the device as a simple RLC circuit shown in Fig. 5(b), where L is series

inductance, C is gate dielectric capacitance, g is AC conductance, and R is series resistance of the substrate and metal contact. From the fitting curve, the circuit parameters are extracted as R=250 Ω, C=3.9 pF, L=11.3 nH, and 1/g=330 kΩ, leading to a cutoff frequency of f_c=163 MHz. Thus, we have verified that the circuit RLC components limit the performance of the modulator. By appropriate optimization of the device circuit design, the operation speed is expected to reach GHz region, so the MICIM plasmonic modulator promises to serve as ultra-compact and ultra-fast optical interconnection.

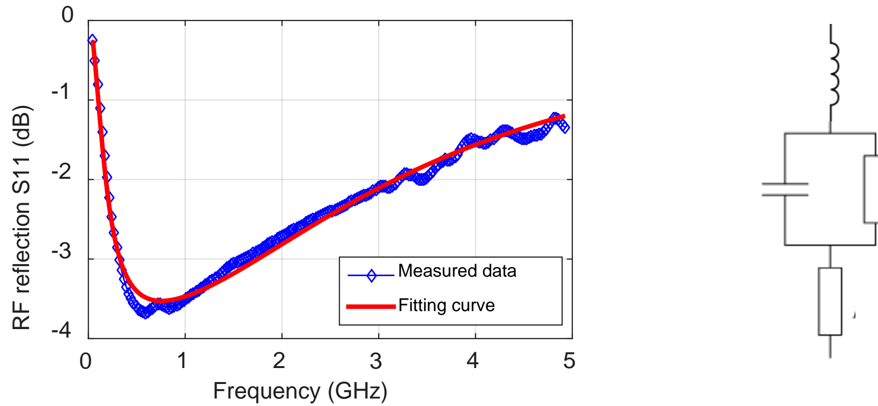

Figure 5. (a) Measured RF reflection coefficient S_{11} and curve fitting. (b) Simple RLC equivalent circuit model of the MICIM plasmonic modulator.

2. Ultra-compact, high-speed dielectric modulator

2.1 Background

Based on the field effect (i.e. carrier accumulation and depletion) within active conductive oxide layer in the MIC and MICIM structures, we have experimentally demonstrated plasmonic EA modulators that have broadband EO response, ultra-compact footprint as well as potentially high operation speed. According to the numerical study of field-effect optical modulators based on ENZ-slot waveguide [11], we can also realize field-effect EA modulation by dielectric waveguide configurations. Compared with plasmonic modulator where light can propagate as surface plasmon polaritons (SPPs) at metal-dielectric surface, dielectric modulator may lose some compactness. However, it promises much easier integration with existing platforms based on CMOS technology. Without metallic components, the optical losses of dielectric modulator will become much smaller. This may solve the problem of the MICIM plasmonic modulator in high input power requirement. Thus, it is worthy of exploring an

efficient and compact dielectric modulator. Besides, we can also utilize optimized design to achieve improved operation speed.

Since 2010 when the EO properties of CO was revealed [15], many works towards CO-based EO modulation have been proposed. However, most of the proposed modulators utilize plasmonic waveguide configurations. Few modulators integrated with dielectric materials have been reported [33, 35]. Zhao et al. reported their numerical study of a high-confinement Si slot-waveguide modulator, in which SiO_2 buffer layer and polysilicon cladding are used to confine EM fields within 10nm ITO film [35]. They also investigated the integration of the slot-waveguide modulator with Si strip waveguides. In Ref. [27], Sorger et al. demonstrated an ITO-based nanophotonic modulator on SOI platform with a modulator length of 3λ, which can reach an extinction ratio of 1 dB/μm over a wide bandwidth range. However, the broadband modulator is actually utilizing the field-effect in an MIC structure. The silicon substrate is mainly used as a waveguide for light interaction with the MIC modulator. Therefore, it is necessary to experimentally demonstrate the operation of a dielectric modulator to facilitate the development of CO-based EO modulators for future integrated photonic circuits.

2.2 Design, modeling, and fabrication

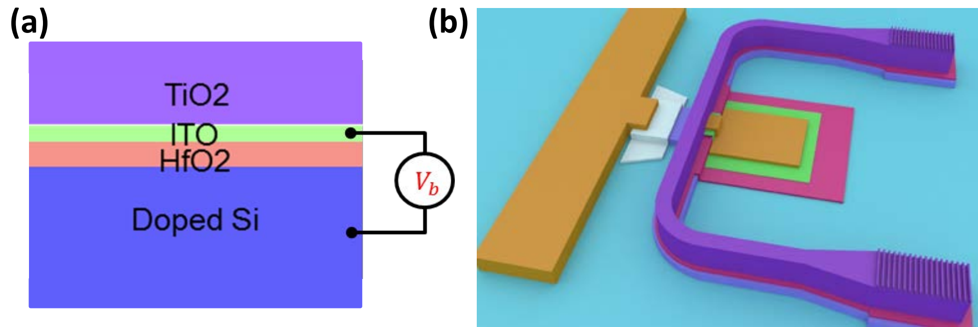

Figure 6. (a) The multi-layer stack of the dielectric modulator. (b) The 3D schematic of the doped Si-insulator-CO dielectric modulator.

The design of the CO-based dielectric modulator is shown in Fig. 6(a). As can be seen, in this dielectric slot waveguide, TiO_2 will serve as the waveguide for guiding light to interact with ITO. ITO slot is embedded between TiO_2 waveguide and doped Si, and again, high k material, HfO_2 is used as gate dielectric. External electric signals will be applied on doped Si and ITO, which stimulates the field effects in the active ITO layer on ITO-HfO_2 interface. Figure 6(b)

illustrates the designed schematic for the device to be fabricated. The device will be fabricated on SOI substrate. In order to reduce optical losses and electrical resistance, only Si in the modulator region will be doped for applying electric signal. Besides, nickel silicide will be used to further reduce contact resistance on doped Si. Since the light coupling in the MICIM plasmonic modulator through a lensed fiber and input/output slits is very poor, we utilize grating couplers in the dielectric modulator. Here, a TiO_2 waveguide with gratings on the two ends is used for light coupling and propagation, where the U-shaped is designed for easy light coupling by using angled fiber arrays. Gold will only be used as contact pads in the device.

Numerical simulation has been done for modulator based on dielectric ENZ-slot waveguide, showing greatly enhanced light absorption at ENZ state. Here, with the designed schematic, we model the whole device for both light coupling and modulation performance. The center wavelength for device operation is set to be 1550 nm, where, according to the simulation, the maximum light coupling efficiency can be achieved with the grating period of 1.4 μm and an incident angle of 28º.

From Fig. 7(a), we can see the schematic model of the device built in Lumerical FDTD solutions. The modulator is located at the center of the U-shaped waveguide. Over each grating coupler is an optical fiber for illuminating or receiving light. In the simulation, light transmission of the device under both original state ($\varepsilon_{\mathrm{ITO}} = 2.53 + j0.11$) and ENZ state ($\varepsilon_{\mathrm{ITO}} = 0.44 + j0.32$) are examined. For the 4-μm-long modulator, the output transmission has a peak value 25.5% for 1555 nm input light when ITO is at original state, and dramatically drops to less than 3% at ENZ state, as can be seen in Fig. 7(b). Therefore, significant light modulation can be expected when the device is switching between original and ENZ state.

Figure 7(c) illustrates the fabrication flow. Starting from 220 nm SOI wafer, the Si layer is first thinned to 120 nm, the designed thickness for Si. Wet oxide furnace growth is used to consume the undesired Si, and the grown thermal oxide then serves as the mask for doping Si layer in the modulator region by solid-source phosphorous diffusion. After stripping the oxide mask in the buffered oxide etch solution, undesired Si layer is removed by plasma etch. In order to optimize electrical contact on doped Si, a thin nickel film is deposited and then annealed by rapid thermal process (RTP) to form nickel silicide, which significantly decreases the resistance of electrical contact films. After that, similar to the plasmonic modulator, layer-by-layer

deposition and liftoff processes are utilized to fabricated the multi-layers of HfO_2 (ALD), ITO (sputtering), TiO_2 (E-beam evaporation) as well as gold (E-beam evaporation). The SEM image of the fabricated device is also shown in Fig. 7(c). The distance between two grating couplers is 127 µm, which matches the spacing of the fiber arrays. The modulator, located in the center of the U-shaped waveguide, is shown in the enlarged image. The modulator width is 1µm, and the minimum designed modulator length is 4 µm. Therefore, the dielectric modulator has a very compact footprint of 4 μm^2.

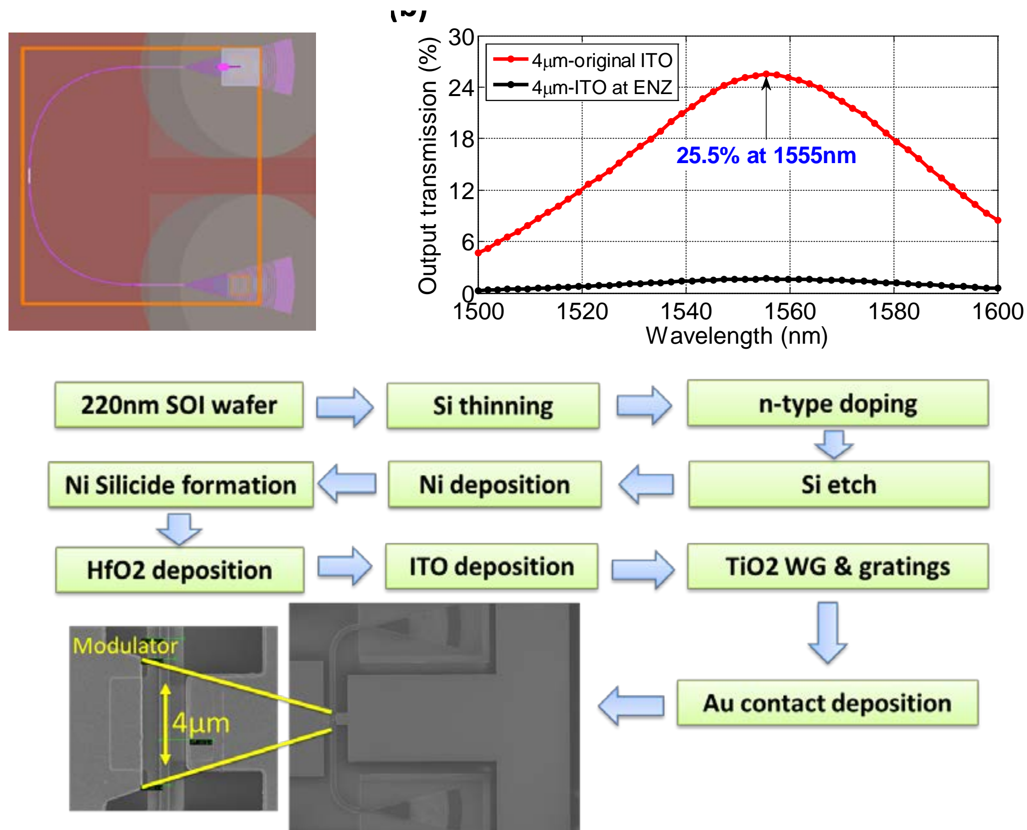

Figure 7. (a) The simulated device schematic in Lumerical FDTD solutions. (b) The output transmission of the modulator at original state and ENZ state. (c). Fabrication flow and SEM images of the device.

2.3 Light coupling and modulation measurement

The experimental setup for the light coupling and modulation measurement is depicted in Fig. 8(a). This is a whole-wafer test setup. A motorized wafer stage is used to hold as well as to precisely control the rotation of the 4-inch wafer. On the right side, four-channel angled fiber

arrays are set above the devices for coupling light in and out. Note that the modulator can only work with TM-polarized light, so the input light from a tunable laser source (1260 nm to 1520 nm) will first go through polarization control before coupling into the device. The output light is fed into a photodiode which connects an oscilloscope or a spectrum analyzer to examine the light power and modulation response. On the left side is a GSG RF probe, which is paired with a function generator, and used for applying electrical signals on the contact pads of the devices. A microscope, installed with an NIR camera at the top through an adapter, is placed over the device under test (DUT) for observation, alignment, and NIR imaging. From the inset of the figure, we can see an NIR camera picture showing light coupling in (bottom side) and out (top side) of the device. Thus, we have achieved successful light coupling without amplifying input optical signal.

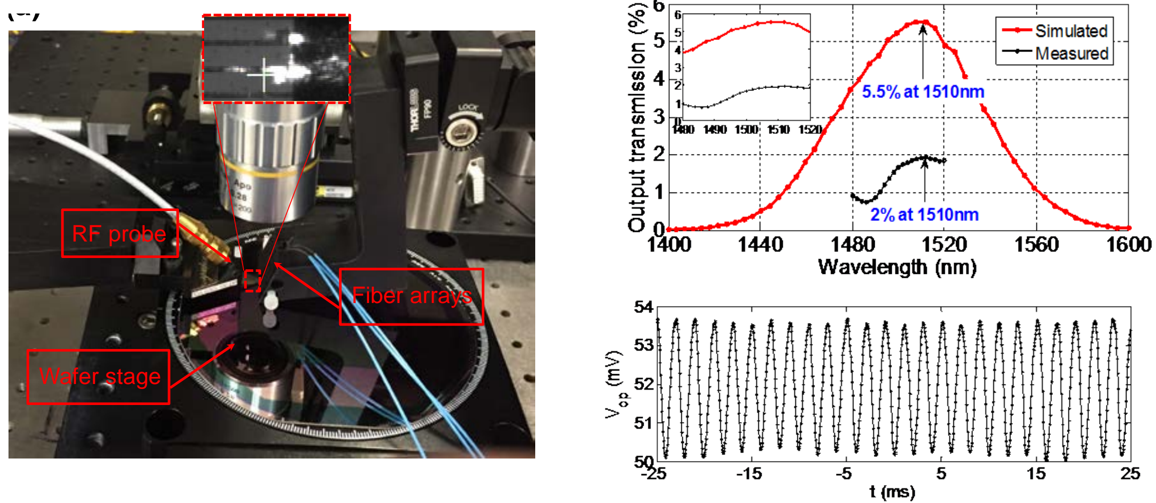

Figure 8. (a) Test setup of light coupling and modulation measurement. (b) Output transmission of the simulated device with updated parameters and the measured output transmission without external electric signal. (c) The output light power waveform of the modulator under a 500 Hz, 11V-V_{pp} electric signal.

Firstly, we investigate the coupling performance of the devices. Due to the wavelength limitation in the laser source, we only plot measured coupling efficiency of the device in the range of 1480 nm to 1520 nm, which shows a peak value of 2% at 1510 nm, which is far less than the simulated result. We update the FDTD simulation results based on the measured film parameters of the fabricated device (thicknesses, indices, dimensional errors), and obtain a peak

5.5% output transmission at the wavelength of 1510 nm, as shown in Fig. 8(b). From the inset, we can see the simulation and test results match well except the magnitude of the coupling efficiency. The degradation should be mainly attributed to the fabrication and measurement imperfection. Note that the highly doped Si contributes to about 0.7% optical loss according to numerical simulation.

Then, with the setup set for maximum output transmission, an AC electric signal is applied on the DUT. With a DC-coupled photodiode (25 MHz bandwidth), the output light power is displayed on the oscilloscope. Figure 8(c) shows the output waveform of the DUT under a 500 Hz, 11V-V_{pp} sinusoidal electric signal, which verifies the EO modulation response. The measured extinction ratio is less than 1dB/μm, which should be mainly due to fabrication imperfections.

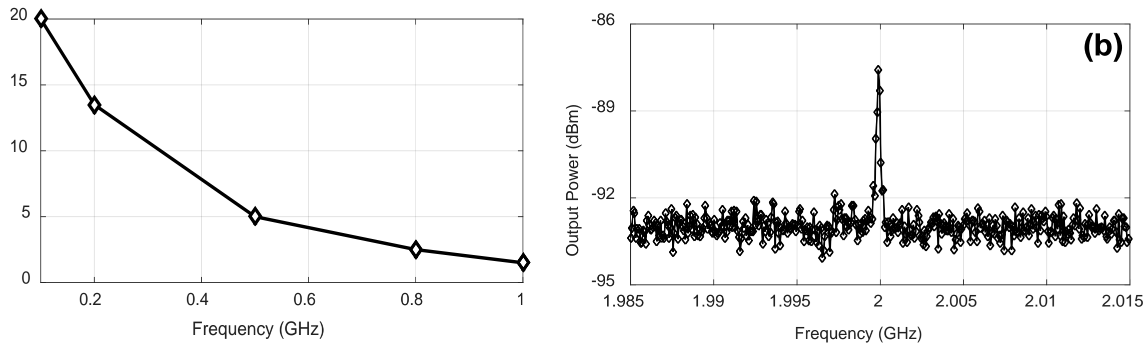

Figure 9. (a) Modulation depth versus frequency measured by a spectrum analyzer. (b) Spectrum analyzer measurement showing optical intensity modulation at 2 GHz.

To investigate the operation speed of the dielectric modulator, an AC-coupled InGaAs photodiode with 10 GHz bandwidth is utilized. The output signal is then analyzed by a high speed (up to 13.2 GHz) spectrum analyzer, where an intensity peak can be observed at certain modulating frequencies. Note that the measurements are taken under the optimum coupling condition (λ = 1510 nm). The amplitude of the peak represents the modulation depth. In Fig. 9(a), the modulation depth of the device under 11V-V_{pp} electric signal is plotted with respect to different modulating frequencies. Clearly, EA modulation at GHz has been successfully achieved. Here, we have obtained an AC modulation depth of 2.5 dB/μm (for 8-μm long modulator waveguide) at 100 MHz. The modulation depth decays with increasing frequency, showing that

the device has a RC circuit-limited operation speed. In particular, we have achieved a modulation speed of up to 2 GHz, as shown in Fig. 9(b).

2.4 Circuit analysis

Due to the RC-limited operation speed exhibited in the dielectric modulator, we again conduct circuit analysis to identify the limitation factors. The measured S_{11} data as a function of frequency is shown as black diamonds in Fig. 10. From the figure, the S_{11} value decreases to -2 dB at 3.2 GHz, and bounces back a little after a certain frequency. We fit the curve by using the same simple RLC equivalent circuit model as the plasmonic modulator (Fig. 9(a)). From the fitting curve, the circuit parameters are extracted as L=108 pH, C=3.1 pF, R=6.2 Ω, and $1/g$=4.4 kΩ. and the cutoff frequency can be estimated as f_c=8.3 GHz. Compared with the plasmonic modulator, the resistance and parasitic inductance of the device circuit have significantly dropped due to the optimized design of the device circuit. In Fig. 9(b), a more complicated circuit model, which takes the capacitance and conductance of the ITO layer into account, is also well fitted. The real circuit of the device should be much more complicated with many more components. We are still working on developing a realistic model to locate the key components that limit the device performance, and expect to achieve an operation speed of tens of GHz by optimizing the design and fabrication accuracy.

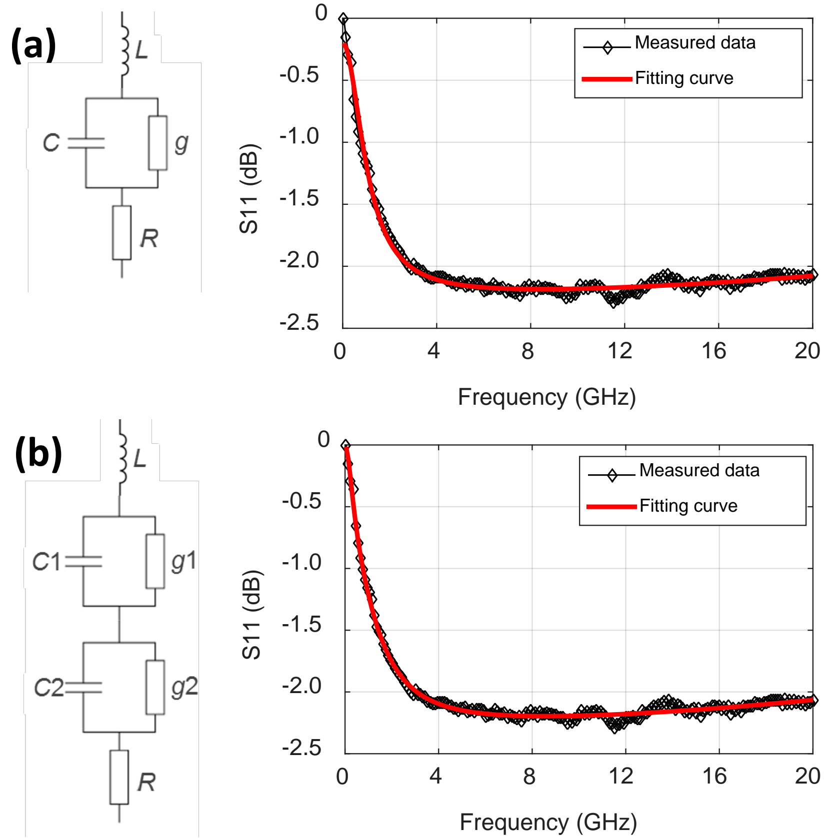

Figure 9. S_{11} measurement and curve fitting of (a) a simple RLC equivalent circuit model of the modulator and (b) a more complicated model.

3. Conclusions

In conclusion, we have experimentally demonstrated ultra-compact and high-speed CO-based EA modulators integrated in plasmonic and dielectric platforms. By utilizing an MICIM structure, where the field effect is enhanced by the double capacitor gating, the plasmonic modulator has an 800-nm long waveguide length, and can achieve an impressive extinction ratio of 3.04 dB/μm. The modulator can work up to 500 MHz according to the measurement. With the U-shaped waveguide and grating coupler design, the doped Si-HfO_2-ITO dielectric modulator exhibits an operation speed of up to 2 GHz at telecommunication wavelengths, which is the first experimental demonstration of GHz operation of CO-based EO modulators. The modulator also has an ultra-compact footprint of 4 μm^2. For both plasmonic and dielectric modulators, the involved fabrication processes are undemanding and CMOS-compatible. According to the circuit analysis, the operation speed of the modulators is mainly limited by circuit RC constant, which

can be boosted to 10s of GHz by optimizations in device design, material properties, and fabrication process. The modulation depth of the dielectric modulator is also expected to be significantly enhanced with the optimization. We can further consider utilizing double capacitor gating scheme in the dielectric modulator to improve modulation efficiency as well as to shrink device dimension. The proposed CO-based modulator devices provide promising candidates for ultra-compact and ultra-fast optical interconnects in future integrated photonic circuits.

References

[1] G. T. Reed, G. Mashanovich, F. Y. Gardes, and D. J. Thomson, "Silicon optical modulators," Nat. Photonics **4**, 518-526 (2010).

[2] B. G. Lee, A. Biberman, J. Chan, and K. Bergman, "High-Performance Modulator and Switches for Silicon Photonic Networks-on-Chip," IEEE J. Sel. Top. Quant. Electron. **16**, 6-22 (2010).

[3] Y. H. Kuo, Y. K. Lee, Y. Ge, S. Ren, J. E. Roth, T. I. Kamins, D. A. B. Miller, and J. S. Harris, "Strong quantum-confined Stark effect in germanium quantum-well structures on silicon," Nature **437**, 1334-1336 (2005).

[4] F. G. Della Corte, S. Rao, M. A. Nigro, F. Suriano, and C. Summonte, "Electro-optically induced absorption in α-Si:H/α-SiCN waveguiding multistacks," Opt. Express **16**, 7540-7550 (2008).

[5] J. Liu., M. Beals, A. Pomerene, S. Bernardis, R. Sun, J. Cheng, L. C. Kimerling, and J. Michel, "Waveguide-integrated, ultralow-energy GeSi electro-absorption modulators," Nature Photon. **2**, 433-437 (2008).
[6] H.W. Chen, Y. H. Kuo, and J. E. Bowers, "25Gb/s hybrid silicon switch using a capacitively loaded traveling wave electrode," Opt. Express **18**, 1070-1075 (2010).
[7] Y. Rong, Y. Ge, Y. Huo, M. Fiorentino, M.R.T. Tan, T. Kamins, T.J. Ochalski, G. Huyet, and J.S. Harris, "Quantum-confined Stark effect in Ge/SiGe quantum wells on Si," IEEE J. Sel. Top. Quant. Electron. **16**, 85-92 (2010).
[8] Q. Xu, B. Schmidt, S. Pradhan, and M. Lipson, "Micrometre-scale silicon electro-optic modulator," Nature **435**, 325-327 (2005).
[9] Q. Xu, S. Manipatruni, B. Schmidt, J. Shakya, and M. Lipson, "12.5 Gbit/s carrier-injection-based silicon microring silicon modulators," Opt. Express **15**, 430-436 (2007).
[10] J. Teng, P. Dumon, W. Bogaerts, H. Zhang, X. Jian, X. Han, M. Zhao, G. Morthier, and R. Baets, "Athermal silicon-on-insulator ring resonators by overlaying a polymer cladding on narrowed waveguides," Opt. Express **17**, 14627-14633 (2009).
[11] Z. Lu, W. Zhao and K. Shi, "Ultracompact electro-absorption modulators based on tunable epsilon-near-zero-slot waveguides," *IEEE J. PHOT*., **4**, 735-740(2012).
[12] K. Shi, R. R. Haque, B. Zhao, R. Zhao, and Z. Lu, "Broadband electro-optical modulator based on transparent conducting oxide," *Opt. Lett*. **39**, 4978-4981(2014).
[13] K. Shi, and Z. Lu, "Field-effect optical modulation based on epsilon-near-zero conductive oxide," *Opt. Commun.* **370,** 22-28 (2016)
[14] K. Shi, and Z. Lu, "Ultracompact field-effect plasmonic modulator," FIO, FTu3D. 2, Oct 2016.
[15] E. Feigenbaum, K. Diest, and H. A. Atwater, "Unity-order index change in transparent conducting oxides at visible frequencies," Nano. Lett. **10**, 2111-2116 (2010).
[16] A. Melikyan, N. Lindenmann, S. Walheim, P. M. Leufke, S. Ulrich, J. Ye, P. Vincze, H. Hahn, T. Schimmel, C. Koos, W. Freude, and J. Leuthold, "Surface plasmon polariton absorption modulator," Opt. Express **19**, 8855–8869 (2011).
[17] V. E. Babicheva and A. V. Lavrinenko, "Plasmonic modulator optimized by patterning of active layer and tuning permittivity," Opt. Commun. **285**, 5500–5507 (2012).
[18] A. V. Krasavin and A. V. Zayats, "Photonic signal processing on electronic scales: Electro-optical field-effect nanoplasmonic modulator," Phys. Rev. Lett. **109**, 053901(5) (2012).
[19] V. E. Babicheva, N. Kinsey, G. V. Naik, M. Ferrera, A. V. Lavrinenko, V. M. Shalaev, and A. Boltasseva, "Towards CMOS-compatible nanophotonics: Ultra-compact modulators using alternative plasmonic materials," Opt. Express **21**, 27326–27337 (2013).
[20] A. P. Vasudev, J. Kang, J. Park, X. Liu, and M. L. Brongersma, "Electro-optical modulation of a silicon waveguide with an "epsilon-near-zero" material," Opt. Express **21**, 123–129 (2013).
[21] C. Huang, R. J. Lamond, S. K. Pickus, Z. R. Li, and V. J. Sorger, "A sub-λ-size modulator beyond the efficiency-loss limit," IEEE Photonics J. **5**, 2202411(10) (2013).
[22] J. S. Schildkraut, "Long-range surface plasmon electrooptic modulator," Appl. Opt. **27**, 4587–4590 (1988).
[23] T. Nikolajsen, K. Leosson, and S. I. Bozhevolnyi, "Surface plasmon polariton based modulators and switches operating at telecom wavelengths," Appl. Phys. Lett. **85**, 5833 (2004).
[24] W. Cai, J. S. White, and M. L. Brongersma, "Compact, high-speed and power-efficient electrooptic plasmonic modulators," Nano Lett. **9**, 4403–4411 (2009).

[25] S. Randhawa, S. Lachèze, J. Renger, A. Bouhelier, R. E. de Lamaestre, A. Dereux, and R. Quidant," Performance of electro-optical plasmonic ring resonators at telecom wavelengths," Opt. Express **20**, 2354–2362 (2012).
[26] J. A. Dionne, K. Diest, L. A. Sweatlock, and H. A. Atwater, "PlasMOStor: a metal-oxide-Si field effect plasmonic modulator," Nano Lett. **9**, 897–902 (2009).
[27] V. J. Sorger, N. D. Lanzillotti-Kimura, R. M. Ma, and X. Zhang, "Ultra-compact silicon nanophotonic modulator with broadband response," Nanophotonics, **1**, 17-22(2012).
[28] H. W. Lee, G. Papadakis, S. P. Burgos, K. Chandler, A. Kriesch, R. Pala, U. Peschel, and H. A. Atwater, "Nanoscale Conducting Oxide PlasMOStor," Nano Lett. **14**, 6463–6468 (2014).
[29] A. Melikyan, L. Alloatti, A. Muslija, D. Hillerkuss, P. C. Schindler, J. Li, R. Palmer, D. Korn, S. Muehlbrandt, D. Van Thourhout, B. Chen, R. Dinu, M. Sommer, C. Koos, M. Kohl, W. Freude, and J. Leuthold, "High-speed plasmonic phase modulators," Nat. Photonics **8**, 229–233 (2014).
[30]C. Haffner, W. Heni, Y. Fedoryshyn, J. Niegemann, A. Melikyan, D. L. Elder, B. Baeuerle, Y. Salamin, A. Josten, U. Koch, C. Hoessbacher, F. Ducry, L. Juchli, A. Emboras, D. Hillerkuss, M. Kohl, L. R. Dalton, C. Hafner, and J. Leuthold, "All-plasmonic Mach–Zehnder modulator enabling optical high-speed communication at the microscale," Nat. Photonics **9**, 525–528 (2015).
[31] R. Hunsperger, *Integrated Optics: Theory and Technology* (Springer Science & Business Media, 2009), Chapter 9.
[32] M. Liu, X. Yin, and X. Zhang, "Double-layer graphene optical modulator," Nano Lett. **12**, 1482–1485 (2012).
[33] J. Baek, J.-B. You, and K. Yu, "Free-carrier electro-refraction modulation based on a silicon slot waveguide with ITO," Opt. Express **23**, 15863–15876 (2015).
[34] X. Liu, J. Park, J.-H. Kang, H. Yuan, Y. Cui, H. Y. Hwang, and M. L. Brongersma, "Quantification and impact of nonparabolicity of the conduction band of indium tin oxide on its plasmonic properties," Appl. Phys. Lett. **105**, 181117(5) (2014).
[35] H. Zhao, Y. Wang, A. Capretti, L. D. Negro, and J. Klamkin, "Broadband electroabsorption modulators design based on epsilon-near-zero Indium Tin Oxide," IEEE J. Sel. Topics Quantum Electron. **20**, 192(2015).